Dysregulation of mannose-6-phosphate dependent cholesterol homeostasis in acinar cells mediates pancreatitis

Olga A. Mareninova, Eszter T. Vegh, Natalia Shalbueva, Carli J.M. Wightman, Dustin L. Dillon, Sudarshan Malla, Yan Xie, Toshimasa Takahashi, Zoltan Rakonczay Jr, Samuel W. French,[‡] Herbert Y. Gaisano, Fred S. Gorelick, Stephen J. Pandol, Steven J. Bensinger, Nicholas O. Davidson, David W. Dawson, Ilya Gukovsky, and Anna S. Gukovskaya.

SUPPLEMENTAL MATERIAL

Methods

Experimental pancreatitis in mice. Cerulein-induced (CER-AP) and L-arginine induced (Arg-AP) acute pancreatitis models were performed in 12-week-old C57BL/6 mice that received 7 hourly i.p. injections of 50 μg/kg cerulein or 3 hourly i.p. injections of 3.3 g/kg Arg; controls received physiologic saline injections. Mice were euthanized for analyses 7 hours after the first cerulein or 24 hours after the first Arg injection. Choline deficient, ethionine-supplemented (CDE) pancreatitis was induced in young (~5-weeks old) female mice fed either CDE or control diet. Mice were euthanized 72 hours after the diet initiation. These models have been described in detail (1-7).

In vivo treatments of mice. 12-week-old WT mice were subjected for 4 consecutive days to daily i.p. injections of 20 mg/kg simvastatin (8,9) or 20 mg/kg T0901317 (10); or 10 mg/kg U18666A for 15 days (11). Control mice received vehicle injections. Some of the simvastatin- and T0901317-treated mice were subjected to CER-AP on day 4, as indicated in corresponding figures.

12-week-old *Gnptab*$^{-/-}$ mice were subjected to daily i.p. injections of 20 mg/kg simvastatin or the same dose of T0901317 for 4 or 21 days. Neither treatment changed total cholesterol content in pancreas.

Pancreas subcellular fractionation. Subcellular fractionation of pancreatic tissue was performed by differential centrifugation (7). Pancreata were collected and homogenized in 8 ml of homogenization buffer with 5 full strokes in a Dounce homogenizer, and the nuclei and cell debris sedimented at 150 g. The postnuclear supernatant was centrifuged at 1,300 g, and the pellet collected and referred to as fraction Z. The supernatant was further centrifuged at 12,000 g, and both the 12,000-g pellet (fraction L) and supernatant (fraction C) were collected. Total protein in the fractions was measured by Bradford assay (Bio-Rad). The amounts of total protein in each fraction were consistent across experimental conditions. The quality of subcellular fractionation was evaluated by IB analysis for specific protein markers [this study and Ref. (7)].

Isolation of mouse pancreatic acinar cells and lobules. Pancreatic acinar cells were isolated from mice of both sexes using a standard collagenase digestion procedure (1-6). Pancreatic lobules (~2-mm thick) were excised and incubated at 37 °C in 199 medium containing 0.1 mg/mL soybean trypsin inhibitor (1).

Human pancreas slices were obtained as in (12), from portions of live normal human pancreata from pre-terminal donors that were not used for transplantation and diverted to research (provided by Trillium Gift of Life Network, Toronto, Ontario, year 2020) or from normal portions of pancreatic cancer operations. Pancreas was cut into ~3x3x3 mm pieces and embedded with 37 °C low melting 3.8% agarose gel in extracellular solution containing (mM): 125 NaCl, 2.5 KCl, 1 $MgCl_2$, 2 $CaCl_2$, 1.25 NaH_2PO_4, 26 $NaHCO_3$, 2 sodium pyruvate, 0.25 ascorbic acid, 3 *myo*-inositol, 6 lactic acid, and 7 glucose, and placed on ice to solidify the gel. The gelled tissue blocks were sliced with Vibratome into 120 µm-thick slices; slices were washed with the same extracellular solution, placed in 199 medium containing 0.1 mg/mL soybean trypsin inhibitor, and treated with CCK-8 (CCK) or carbachol for ex-vivo pancreatitis.

Baculoviral transduction. CellLight™ Rab5a-GFP and Rab7a-RFP reagents were added to suspension of isolated mouse acinar cells to reach the final concentration of 30 particles/cell, per manufacturer's protocol. The cells were gently shaken at 37 °C for 1 h to maximize transduction efficiency, cultured for another 16 hours, fixed, and analyzed by confocal microscopy.

Mitochondria isolation and functional assays. Mitochondria were isolated from mouse pancreas and liver in a Ca^{2+}-free medium in the presence of 1 mM EGTA, as in (3-5,13). The value of respiratory control ratio in these preparations, measured in the presence of succinate (quality control parameter), was greater than 3.0.

Mitochondrial membrane potential ($\Delta\Psi m$) was measured in mitochondria suspension (1 mg/ml protein) using a tetraphenyl phosphonium (TPP^+) electrode (3-5,13) in a buffer containing (mM) 250 sucrose, 22 KCl, 22 triethanolamine (pH 7.4), 3 $MgCl_2$, 5 KH_2PO_4, 1 EGTA, supplemented with 0.5% BSA and 10 mM glutamate plus 2 mM malate as the respiratory substrate. An increase in $\Delta\Psi m$ results in TPP^+ uptake by mitochondria and, correspondingly, a decrease in external TPP^+ concentration measured with the TPP^+ electrode. The mitochondrial uncoupler FCCP was added at the end of each experiment to cancel $\Delta\Psi m$ and thus normalize the changes in $\Delta\Psi m$. Variations in the basal $\Delta\Psi m$ values between mitochondria preparations from normal mouse pancreas did not exceed 3%.

Specific activities of individual ETC complexes were measured spectrophotometrically in homogenates of isolated mitochondria or submitochondrial particles, as in (14).

Oxygen consumption rates (OCR) were measured in live acinar cells using Seahorse XFe96, as in (15). As shown in Figure 7, the decrease in OCR upon injection of the ATP synthase inhibitor oligomycin represents a portion of basal respiration that is used to drive ATP production (ATP-linked). Addition of the uncoupler FCCP, which stimulates the respiratory chain to operate at maximum capacity, yields the value of maximal OCR. The combination of complex I inhibitor rotenone and complex III inhibitor antimycin A is added to shut down mitochondrial respiration, providing the contribution of non-mitochondrial respiration to correct for. In all within-set

experiments we used the same volume of cell suspension with the same amount of protein; and partial oxygen pressure was monitored to ensure its stability in the cell suspension.

IB analysis was done as in (1-7,15). Immunoblots were developed using enhanced chemiluminescence detection kit (Pierce), and band intensities were quantified by densitometry using FluorChem HD2 imaging system (Alpha Innotech/ProteinSimple).

Fluorescence and light microscopy were utilized as described in (1-7,15). Pancreatic tissue was cut into ~3x3x3 mm pieces and fixed overnight at 4 °C with 4% (w/v) methanol-free paraformaldehyde in 0.1 M phosphate buffer. Tissue pieces were then equilibrated in 15% sucrose-phosphate buffer, embedded in Tissue-Tek OCT compound, and stored at -80 °C. For paraffin embedding, pancreatic tissue pieces were fixed in 10% buffered formaldehyde. Acinar cell pellets were fixed for 20 min at room temperature in 4% (w/v) paraformaldehyde in 0.1 M phosphate buffer.

Fixed-frozen or paraffin-embedded pancreas and liver tissue sections and fixed cells were processed as in (1-7) and immunolabeled by incubating overnight at 4 °C with primary antibodies, followed by incubation with secondary antibodies conjugated with FITC or Texas Red. Nuclei were counterstained with DAPI or NucRed 647.

Staining for neutral lipids and free cholesterol was performed by incubation of fixed-frozen tissue sections or fixed cells with, respectively, 2 μg/ml BODIPY493/503 for 45 min or 100 μg/ml filipin for 2 h at room temperature. For double labeling, BODIPY493/503 or filipin were applied after fixed-frozen tissue or cell sections incubated with primary and secondary antibodies.

To label acidic organelles, acinar cells were incubated with 100 nM LysoTracker Deep Red for 15 min at RT, washed, and fixed for 20 min in 4% (w/v) paraformaldehyde in 0.1 M phosphate buffer at room temperature.

For trypsinogen activation peptide (TAP) immunolabeling, pancreatic lobules were fixed with 2% paraformaldehyde and 0.05% glutaraldehyde in PBS, and processed as in (7,16).

All fluorescence images were acquired with a Zeiss LSM710 confocal microscope using x63 objective and preset within-experiment image acquisition settings. Quantitative fluorescence analysis was performed with Volocity software (PerkinElmer). Overlap between 2 fluorescent labels was measured using Manders-Costes coefficient. Pearson's colocalization coefficient was calculated if both immunolabeled proteins had the same (e.g. "dotted") staining pattern.

Immunohistochemical detection of the infiltrating inflammatory cells was performed on paraffin-embedded pancreas sections using streptavidin-biotin immunoenzymatic antigen detection system, as in (1,2).

Transmission electron microscopy. For electron microscopy (1-3,7), the tissue was cut into 1-mm cubes and fixed overnight at 4 °C in 2.5% glutaraldehyde, 150 mM sodium cacodylate (pH 7.4). After postfixation in 1% OsO_4 followed by uranyl acetate, the tissue was dehydrated in ethanol and embedded in epoxy resin. 100-nm-thick sections were examined (S.W.F.) in a Hitachi-600 electron microscope.

qPCR. Total RNA was isolated from tissue or cells using QIAGEN RNeasy Plus kit according to the manufacturer's instructions, quantified in NanoDrop, and converted to cDNA with high-capacity cDNA reverse transcription kit. KAPA SYBR FAST qPCR Master Mix kit and a LightCycler 480 were used for quantitative PCR. Fold change related to the control group was calculated using the $2^{\Delta\Delta Ct}$ method with *Rplp0/36B4* as the reference gene. Primers are available upon request.

Transferrin-Alexa594 (Tf-594) internalization assay. Mouse acinar cells were incubated for 2 h in serum-free 199 medium, pulsed with the fluorescently labeled Tf-594 (25 μg/ml) for 30 min on ice, washed with PBS, transferred to 37 ˚C, and chased for 3, 30, and 90 min. At these time points, cells were placed on ice, fixed, and analyzed with confocal microscopy.

Measurement of protease and lipase activities. Activities of cathepsin (Cat) B and L, caspase-3, trypsin, and lysosomal acid lipase (LAL) were measured in pancreatic tissue or cell homogenates and subcellular fractions with fluorogenic assays using substrates specific for CatB

(Z-Arg-Arg-AMC), CatL (Z-Phe-Arg-AMC), caspase-3-like (Z-VAD-fmk), trypsin (Boc-Gln-Ala-Arg-AMC), as previously described (1-4,6,7); and for LAL (4-methylumbelliferyl oleate), as in (17). In measurements of CatL activity, the assay buffer also contained 50 μM CA-074me, a CatB inhibitor. LAL activity was measured in the absence and presence of the LAL inhibitor lalistat (100 μM) as the difference between these values (17).

Cholesterol and triglyceride assays. Total cholesterol content was measured with Cholesterol Assay kit per manufacturer's instructions. Samples of mouse pancreas and liver, cell pellet homogenates, subcellular fractions, isolated mitochondria, and serum were diluted in the reaction buffer containing cholesterol probe and incubated at 37 °C for 1 h in the dark. To measure total cholesterol, the samples were subjected to digestion with cholesterol esterase. To measure non-esterified cholesterol, the esterase was omitted from the assay.

Triglycerides (TAG) content was measured using Triglyceride Assay kit. Tissue samples were homogenized in 10% (w/v) NP-40 aqueous solution, subjected to two heating/cooling cycles to solubilize triglycerides, and centrifuged to remove insoluble material. Supernatants were diluted with water and mixed with lipase-containing reaction mix per manufacturer's instructions.

For measurement of free fatty acids (FFA), lipids were extracted from tissue or isolated mitochondria using chloroform:methanol (2:1 v/v). FFA content was measured by enzymatic assay using HR kits.

Fluorescence intensity (for cholesterol) and absorbance (for TAG) were measured in a Tecan microplate reader. Each measurement was in duplicate, and the values were normalized per mg total protein in the sample.

LDL uptake was measured as in (18). Isolated acinar cells were incubated in serum-free 199 medium for 2 h at RT, washed with PBS, and incubated with 5 μg/mL DyLight550-labeled LDL for additional 2 h at 37 °C. Then, cells were resuspended in a lysis buffer; cell debris were removed by centrifugation, and the fluorescent signal in cell lysate was measured in a Typhoon imager at Ex/Em = 540/570 nm and normalized to total protein in the lysate.

Cytokine/chemokine measurements. Samples were prepared as in (19). Briefly, tissue was homogenized in the presence of 25 U/ml benzonase endonuclease, and protease inhibitors cocktail and incubated on ice, and cell debris were removed by centrifugation at 4 °C. Cytokines and chemokines were measured in the supernatants with Luminex® 200™ Multiplexing Instrument using mouse 32-plex Cytokine/Chemokine panel, and normalized per total protein in the sample.

Pancreatitis responses were measured as previously described (1-7). Serum amylase and lipase were measured in a Hitachi 707 analyzer. Acinar cell vacuolization and necrosis were quantified on H&E stained pancreatic tissue sections; at least 1000 acinar cells/mouse were analyzed in several high-power fields. ATP was measured in tissue homogenates using bioluminescence assay (3-5).

Amylase secretion was assayed as in (1,2), by measuring the amount of amylase both in the incubation medium and in cells with the Phadebas amylase assay kit.

Serum markers of liver damage. Plasma concentrations of aspartate aminotransferase and alanine aminotransferase were determined by corresponding assay kits per manufacturer's instructions.

Methods References

1. Mareninova OA, et al. Lysosome associated membrane proteins maintain pancreatic acinar cell homeostasis: LAMP-2 deficient mice develop pancreatitis. Cell Mol Gastroenterol Hepatol. 2015;1(6):678-94.
2. Mareninova OA, et al. Transgenic expression of GFP-LC3 perturbs autophagy in exocrine pancreas and acute pancreatitis responses in mice. Autophagy. 2020;16(11):2084-97.
3. Biczo G, et al. Mitochondrial dysfunction, through impaired autophagy, leads to endoplasmic reticulum stress, deregulated lipid metabolism, and pancreatitis in animal models. Gastroenterology. 2018;154(3):689-703.

4. Mukherjee R, et al. Mechanism of mitochondrial permeability transition pore induction and damage in the pancreas: inhibition prevents acute pancreatitis by protecting production of ATP. Gut. 2016;65(8):1333-46.
5. Shalbueva N, et al. Effects of oxidative alcohol metabolism on the mitochondrial permeability transition pore and necrosis in a mouse model of alcoholic pancreatitis. Gastroenterology. 2013;144(2):437-46 e6.
6. Mareninova OA, et al. Cell death in pancreatitis: caspases protect from necrotizing pancreatitis. J Biol Chem. 2006;281(6):3370-81.
7. Mareninova OA, et al. Impaired autophagic flux mediates acinar cell vacuole formation and trypsinogen activation in rodent models of acute pancreatitis. J Clin Invest. 2009;119(11):3340-55.
8. Dong W, Vuletic S, and Albers JJ. Differential effects of simvastatin and pravastatin on expression of Alzheimer's disease-related genes in human astrocytes and neuronal cells. J Lipid Res. 2009;50(10):2095-102.
9. Ziros P, et al. Hepatic Fgf21 expression is repressed after simvastatin treatment in mice. PloS one. 2016;11(9):e0162024.
10. Heckmann BL, et al. Liver X receptor alpha mediates hepatic triglyceride accumulation through upregulation of G0/G1 Switch Gene 2 expression. JCI Insight. 2017;2(4):e88735.
11. Takano T, et al. Augmentation of DHCR24 expression by hepatitis C virus infection facilitates viral replication in hepatocytes. J Hepatol. 2011;55(3):512-21.
12. Liang T, et al. Ex vivo human pancreatic slice preparations offer a valuable model for studying pancreatic exocrine biology. J Biol Chem. 2017;292(14):5957-69.
13. Odinokova IV, et al. Mechanisms regulating cytochrome c release in pancreatic mitochondria. Gut. 2009;58(3):431-42.
14. Barrientos A. In vivo and in organello assessment of OXPHOS activities. Methods. 2002;26(4):307-16.

15. Maertin S, et al. Roles of autophagy and metabolism in pancreatic cancer cell adaptation to environmental challenges. Am J Physiol Gastrointest Liver Physiol 2017;313:G524-G536.

16. Otani T, Chepilko SM, Grendell JH, and Gorelick FS. Codistribution of TAP and the granule membrane protein GRAMP-92 in rat caerulein-induced pancreatitis. Am J Physiol. 1998; 275(5):G999-G1009.

17. Tuohetahuntila M, et al. Lysosome-mediated degradation of a distinct pool of lipid droplets during hepatic stellate cell activation. J Biol Chem. 2017;292(30):12436-48.

18. Loregger A, Nelson JK, and Zelcer N. Assaying low-density-lipoprotein (LDL) uptake into cells. Methods Mol Biol. 2017;1583:53-63.

19. Staples E, Ingram RJ, Atherton JC, Robinson K. Optimising the quantification of cytokines present at low concentrations in small human mucosal tissue samples using Luminex assays. J Immunol Methods. 2013;394(1-2):1-9.

Supplemental Table 1

Human pancreatitis tissue

Code	Age/Sex	Procedure	Diagnosis/Reason for surgery	Presumed explanation for pancreatitis in sampled section
CP1	66/F	Whipple	Autoimmune pancreatitis, type 2	Autoimmune pancreatitis, type 2
CP2	73/F	Enucleation	Well differentiated Pancreatic Neuroendocrine Tumor, Grade2	Pancreatitis associated with obstruction caused by PNET
CP3	61/M	Whipple	Chronic pancreatitis (unclear etiology)	Chronic pancreatitis of unclear etiology (no support for autoimmune)
CP4	71/M	Whipple	Chronic pancreatitis (unclear etiology) presenting as mass lesion	Chronic pancreatitis of unclear etiology (no support for autoimmune)
CP5	21/F	Distal pancreatectomy	Chronic pancreatitis with duct stricture (unclear etiology)	Chronic pancreatitis with duct stricture, unclear etiology (no support for autoimmune)
CP6	69/F	Distal pancreatectomy	Low grade IPMN	Pancreatitis associated with obstruction caused by IPMN
CP7	46/M	Whipple	Chronic pancreatitis (unclear etiology)	Chronic pancreatitis of unclear etiology (no support for autoimmune)
CP8	67/M	Distal pancreatectomy	Benign congenital cyst	Pancreatitis associated with obstruction caused by benign congenital cyst
CP9	75/F	Whipple	Well differentiated Pancreatic Neuroendocrine Tumor, Grade1	Pancreatitis associated with obstruction caused by PNET
CP10	59/M	Whipple	Chronic pancreatitis (unclear etiology)	Chronic pancreatitis of unclear etiology (no support for autoimmune)
CP11	71/M	Whipple	Moderately differentiated pancreatic adenocarcinoma	Pancreatitis associated with obstruction caused by PDAC

No pancreatitis tissue

Code	Age/Sex	Procedure	Diagnosis/ Reason for surgery	Sampled section
NP1	60/M	Whipple	Ampullary adenocarcinoma	Uninvolved histologically normal pancreas
NP2	80/M	Whipple	Ampullary adenocarcinoma	Uninvolved histologically normal pancreas
NP3	40/F	Whipple	Well differentiated Pancreatic Neuroendocrine Tumor, Grade 1	Uninvolved histologically normal pancreas
NP4	68/M	Distal pancreatectomy	Well differentiated Pancreatic Neuroendocrine Tumor, Grade 1	Uninvolved histologically normal pancreas
NP5	51/M	Whipple	Well differentiated Pancreatic Neuroendocrine Tumor, Grade 1	Uninvolved histologically normal pancreas
NP6	39/F	Whipple	Well differentiated Pancreatic Neuroendocrine Tumor, Grade 1	Uninvolved histologically normal pancreas
NP7	67/M	Distal pancreatectomy	Well differentiated Pancreatic Neuroendocrine Tumor, Grade 1	Uninvolved histologically normal pancreas
NP8	40/M	Whipple	Well differentiated Pancreatic Neuroendocrine Tumor, Grade 1	Uninvolved histologically normal pancreas
NP9	41/M	Distal pancreatectomy	Well differentiated Pancreatic Neuroendocrine Tumor, Grade 2	Uninvolved histologically normal pancreas
NP10	71/M	Whipple	Well differentiated Pancreatic Neuroendocrine Tumor, Grade 2	Uninvolved histologically normal pancreas

Note: All samples were taken > 1 cm away from any associated lesion. All samples were evaluated and placed in formalin fixative at the time of intraoperative evaluation.

Supplemental Figures

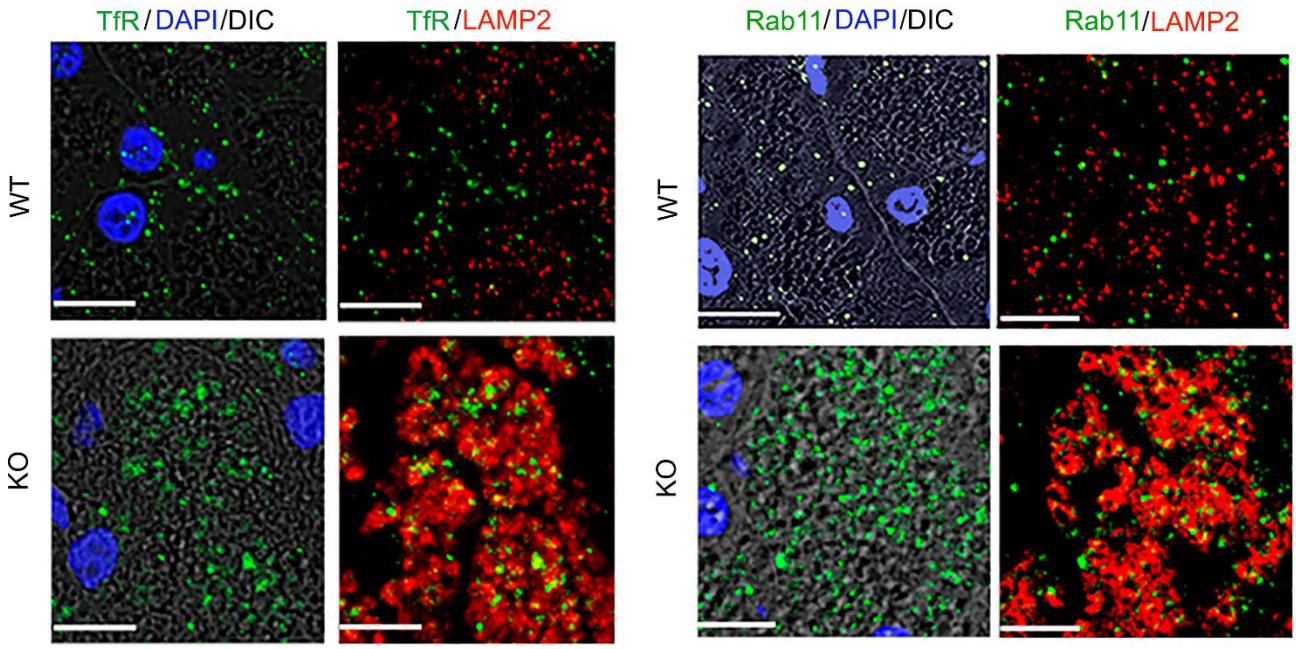

Figure S1. Immunofluorescence colocalization of markers of early (TfR) or recycling (Rab11) endosomes with the LE/Ly marker LAMP2 in *Gnptab*$^{-/-}$ pancreas. Quantitative analysis of these images is presented in Figure 3E-H.

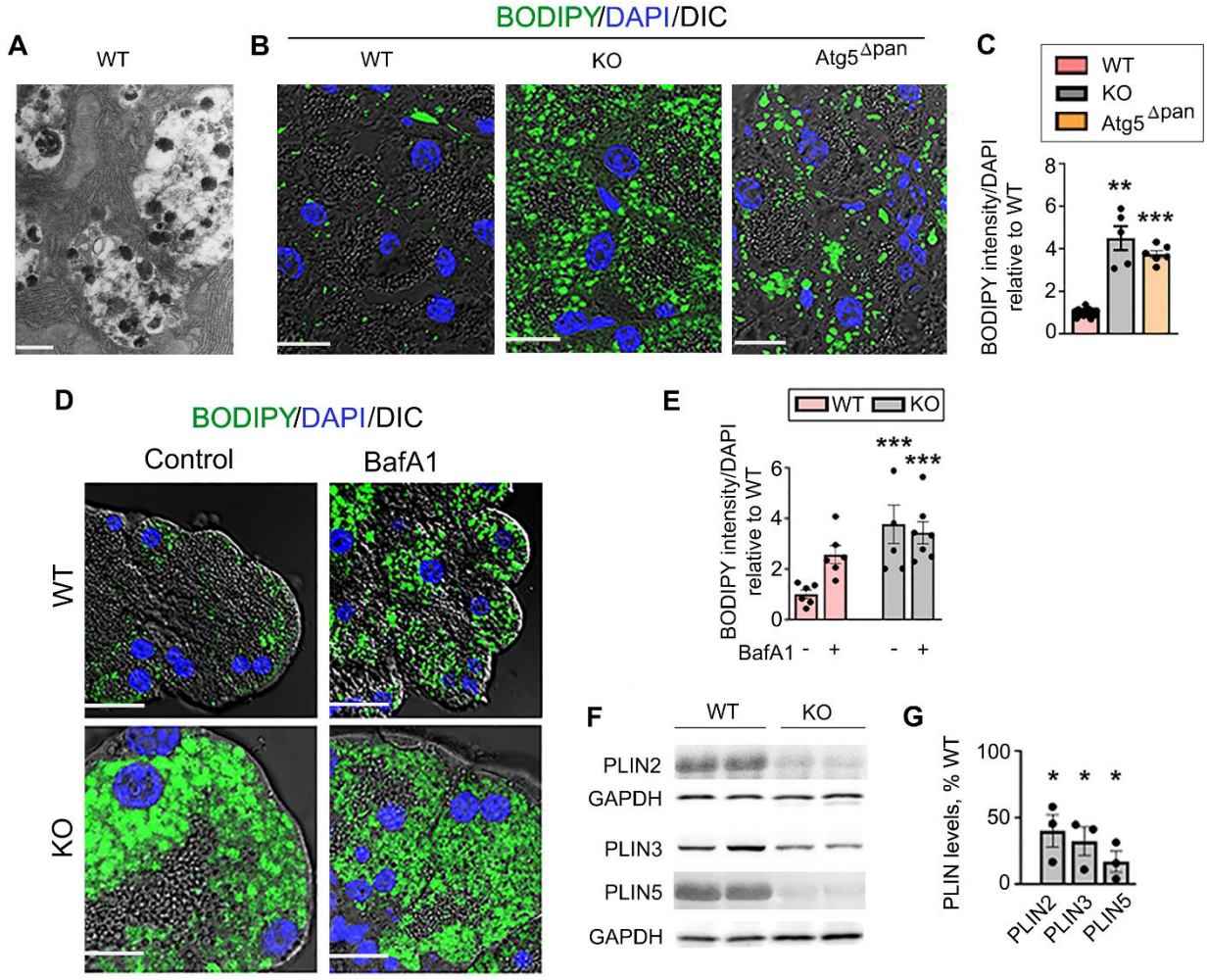

Figure S2. Neutral lipids accumulate in LE/Ly and autophagic compartments of *Gnptab*$^{-/-}$ pancreas. Characteristics of neutral lipid metabolism were measured in (**A**–**C**,**F**,**G**) pancreatic tissue of WT, *Gnptab*$^{-/-}$ (KO) and *Atg5*$^{\Delta pan}$ mice, and (**D,E**) WT and KO acinar cells treated with Bafilomycin A1 (BafA1; 20 nM). (**A**) EM showing lipid inclusions in KO pancreas. (**B**–**E**) Tissue or cells were stained with BODIPY 493/503 for neutral lipids; BODIPY fluorescence intensity was quantified with Volocity software, normalized to the number of nuclei (DAPI) in the field, and expressed relative to WT control. In (**C**), each symbol corresponds to 20-30 cells in a different field (n=5-6 fields from 3 mice of each strain). In (**E**), each symbol corresponds to 10-15 cells in a different field (n=6-7 fields from 3 WT and 3 KO cell preparations). (**F**,**G**) Perilipins (PLINs) were analyzed by immunoblot; their band intensities were densitometrically quantified, normalized to GAPDH in the same sample and, further, to WT. Each symbol represents an individual mouse (n=3 mice of each strain). Each lane on tissue IB represents an individual mouse; ERK1/2 or GAPDH serve as loading control. Values are mean ± SEM. *p<0.05, **p<0.01, ***p<0.001 vs the same parameter in WT tissue or (**E**) control/untreated WT cells. Significance was determined by 2-tailed Student's *t* test (**G**) or 1-way ANOVA followed by Tukey's multiple comparisons test (**C**,**E**). Scale bars: 5 µm (**A**) and 10 µm (**B**,**D**).

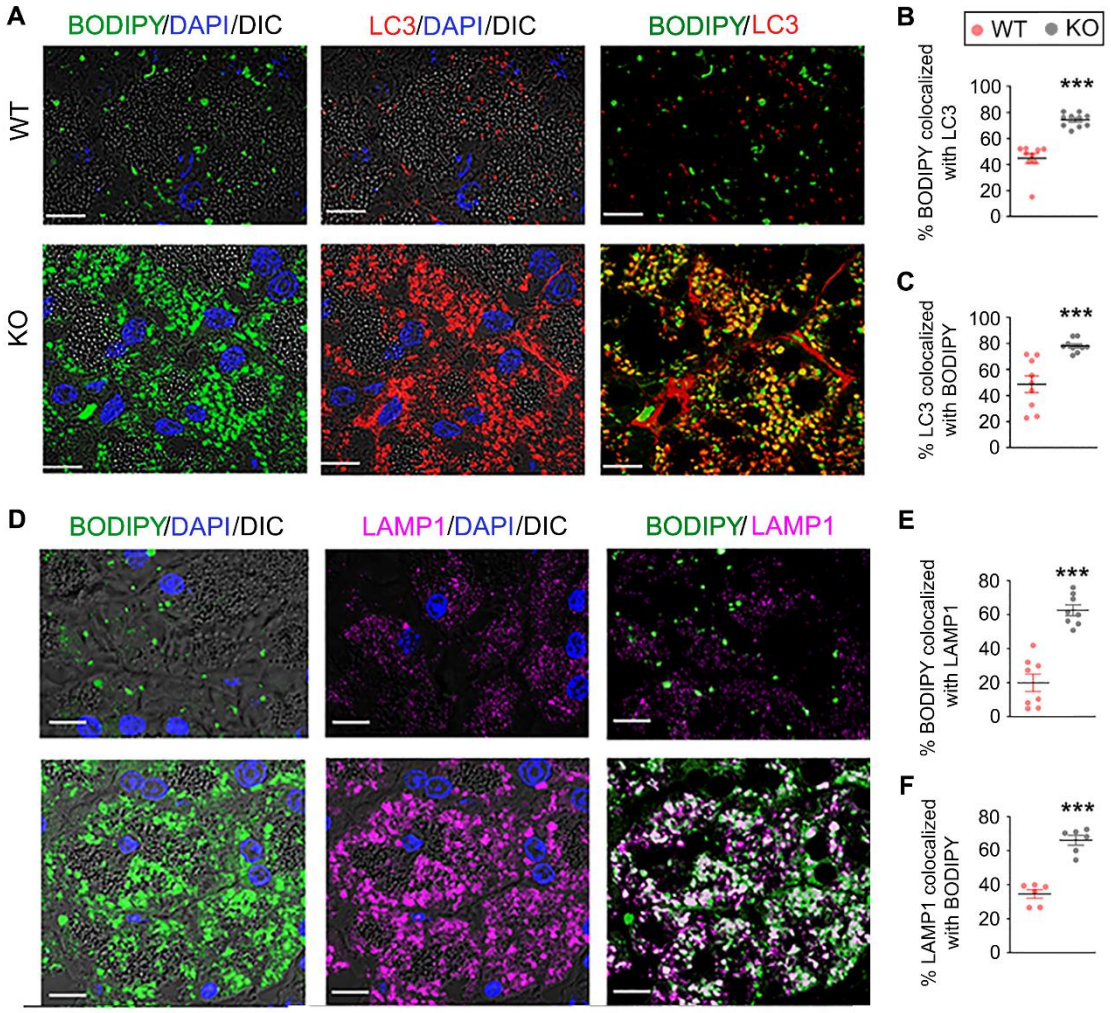

Figure S3. Colocalization of neutral lipids stain with markers of autophagic (LC3 puncta) and LE/Ly (LAMP1) compartments in *Gnptab*$^{-/-}$ pancreas. WT and KO pancreatic tissue sections were stained with BODIPY 493/503 for neutral lipids. Colocalization of BODIPY with LC3 (**A**–**C**) or LAMP1 (**D**–**F**) was quantified with Volocity software using Manders-Costes coefficients. Each symbol corresponds to 20-30 cells in a different field (n=6-10 fields from 3 mice of each strain). Values are mean ± SEM. ***p<0.001 vs the same parameter in WT tissue; 2-tailed Student's *t* test. Scale bars: 10 µm.

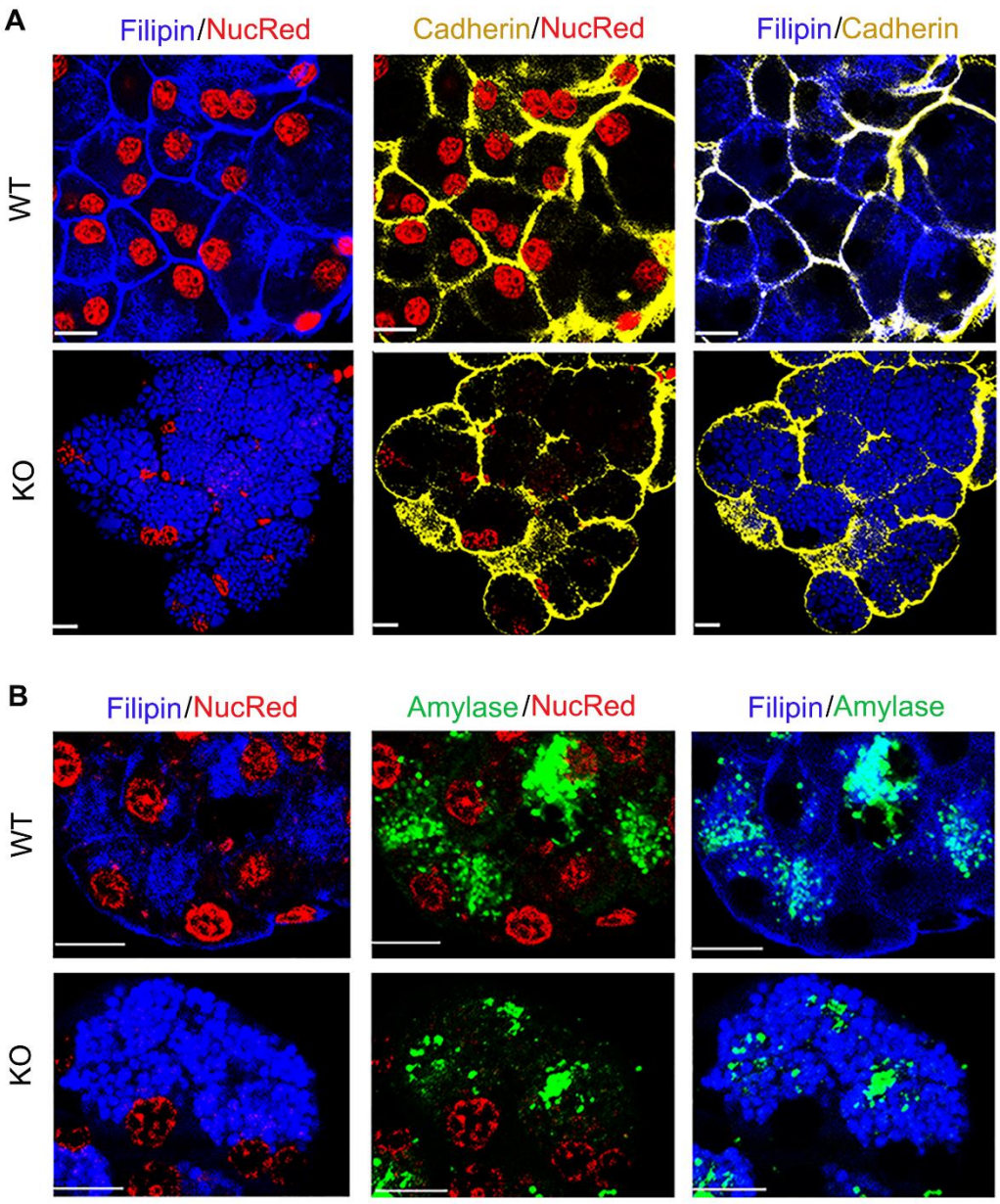

Figure S4. *Gnptab* ablation depletes non-esterified (free) cholesterol in acinar cell plasma membrane and zymogen granules. Colocalization of the free-cholesterol probe filipin with markers of (**A**) plasma membrane (cadherin; pan-cadherin Ab) and (**B**) zymogen granules (amylase) in acinar cells was visualized with confocal microscopy. Quantitative analysis of these images is presented in Figure 4J-L. Scale bars: 10 µm.

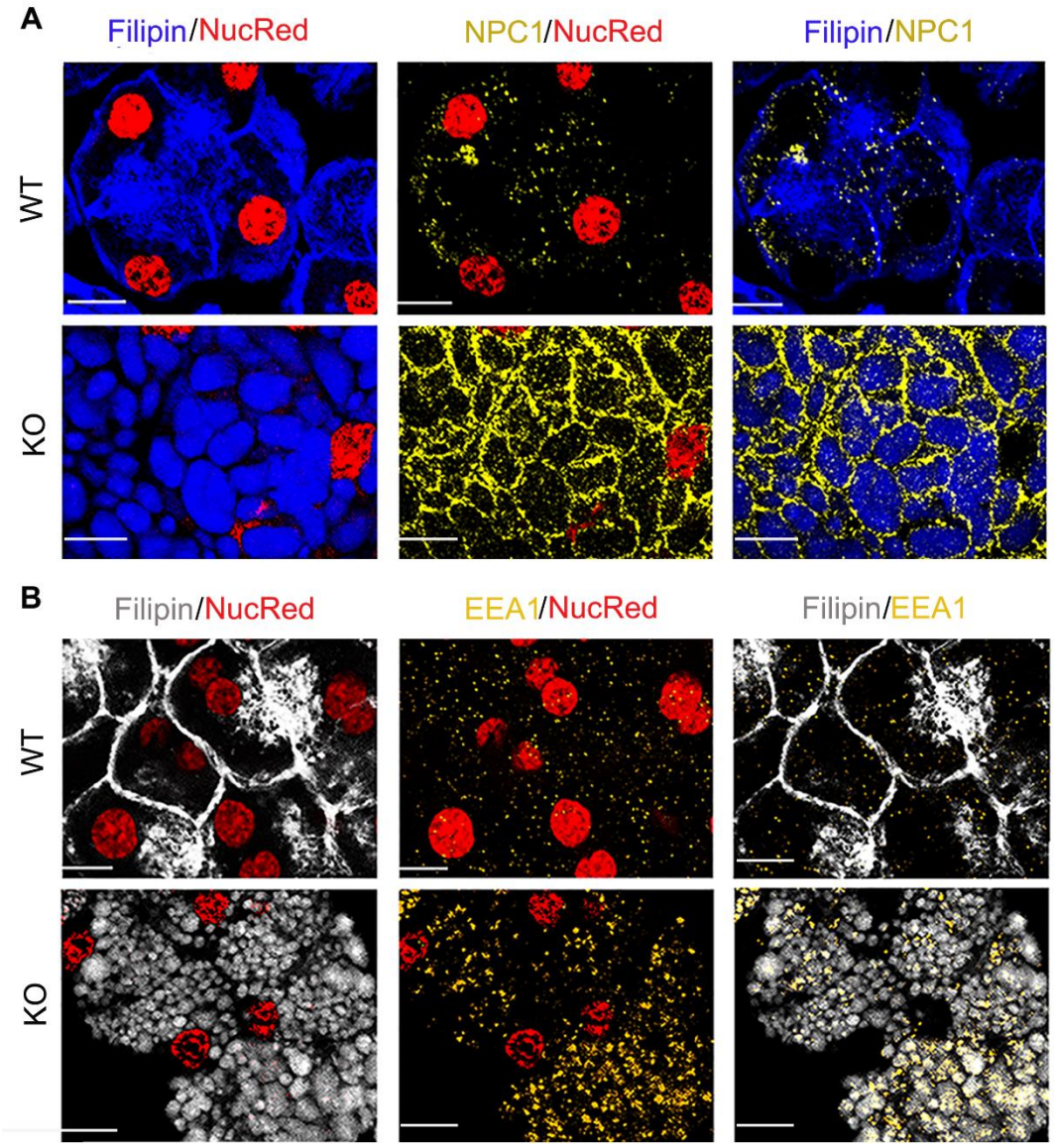

Figure S5. *Gnptab* ablation perturbs non-esterified (free) cholesterol localization in acinar cell endolysosomal system. Filipin colocalization with markers of (**A**) LE/Ly (NPC1) and (**B**) early endosomes (EEA1) in acinar cells was visualized with confocal microscopy. Quantitative analysis of these images is presented in Figure 4M,N. Scale bars: 10 µm.

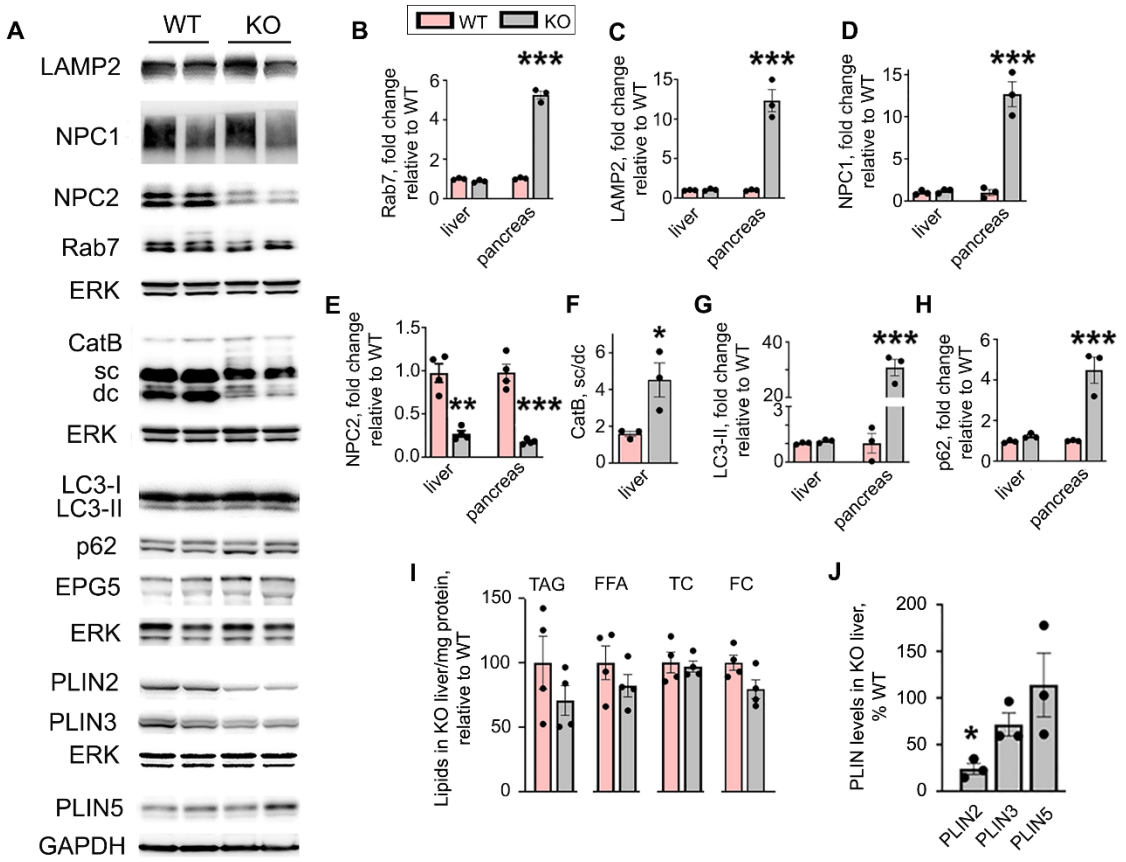

Figure S6. *Gnptab* ablation does not perturb the endolysosomal system and does not alter cholesterol content in liver. (**A**–**H**,**J**) IB analysis of markers/mediators of late endosomes/lysosomes (LAMP2, Rab7, CatB), cholesterol trafficking (NPC1, NPC2), autophagy (LC3, p62, EPG5), and lipid droplets (PLINs). In (**A**), CatB immunoblot shows bands corresponding to the proform, intermediate/single-chain (sc) and mature/double-chain (dc) forms. (**B**–**H**,**J**) Protein band intensities in liver (**A**) and pancreas (see immunoblots in Figures 1, 2, 4, and S2) were densitometrically quantified, normalized to ERK or GAPDH in the same sample, and expressed relative to WT. (**I**) Triglycerides (TAG), free fatty acids (FFA), total (TC) and free (FC) cholesterol contents in liver were measured by enzymatic assays. Values are mean ± SEM from 3-4 mice of each strain; each symbol represents an individual mouse. *p<0.05, **p<0.01, ***p<0.001 vs the same tissue in WT. Significance was determined by 2-tailed Student's *t* test (**F**,**J**) or 1-way ANOVA followed by Tukey's multiple comparisons test (**B**–**E**,**H**).

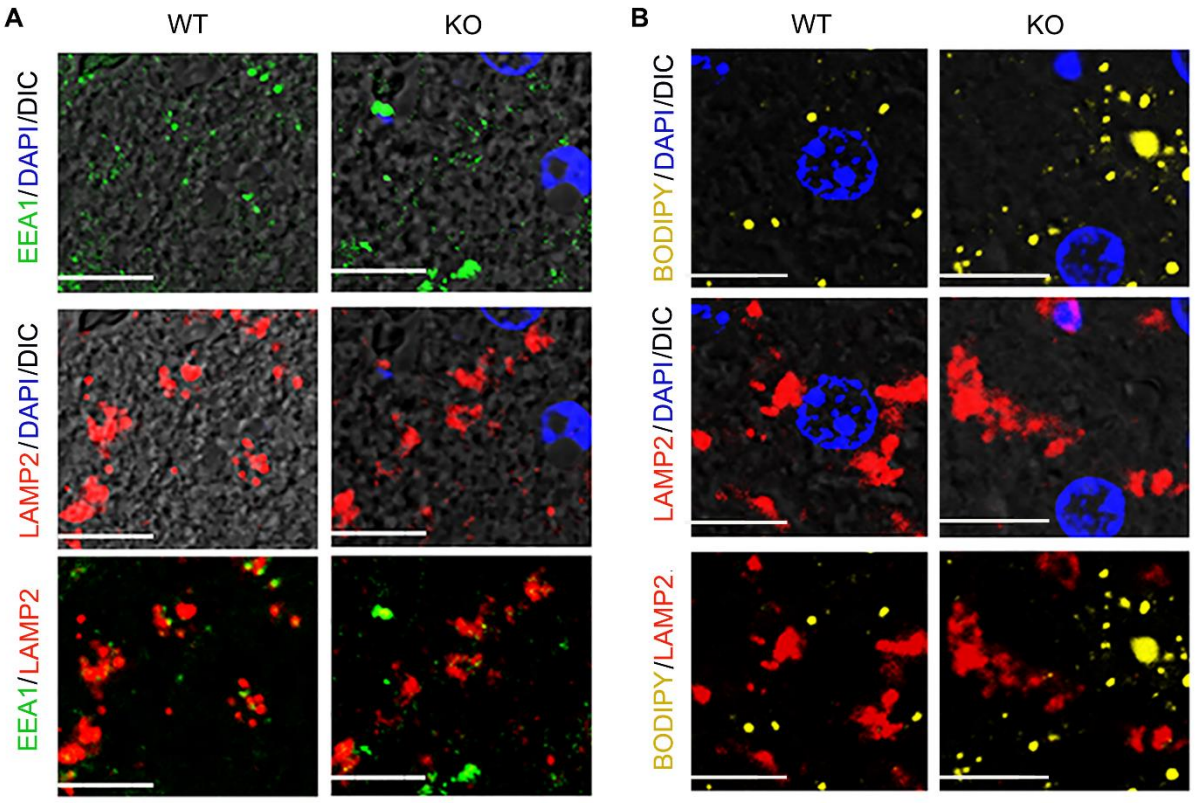

Figure S7. *Gnptab* ablation does not increase colocalization of early endosomes and neutral lipids with LE/Ly compartment in liver. Immunolabeling for LAMP2 and EEA1, and BODIPY 493/503 staining for neutral lipids in KO liver. Scale bars: 10 µm.

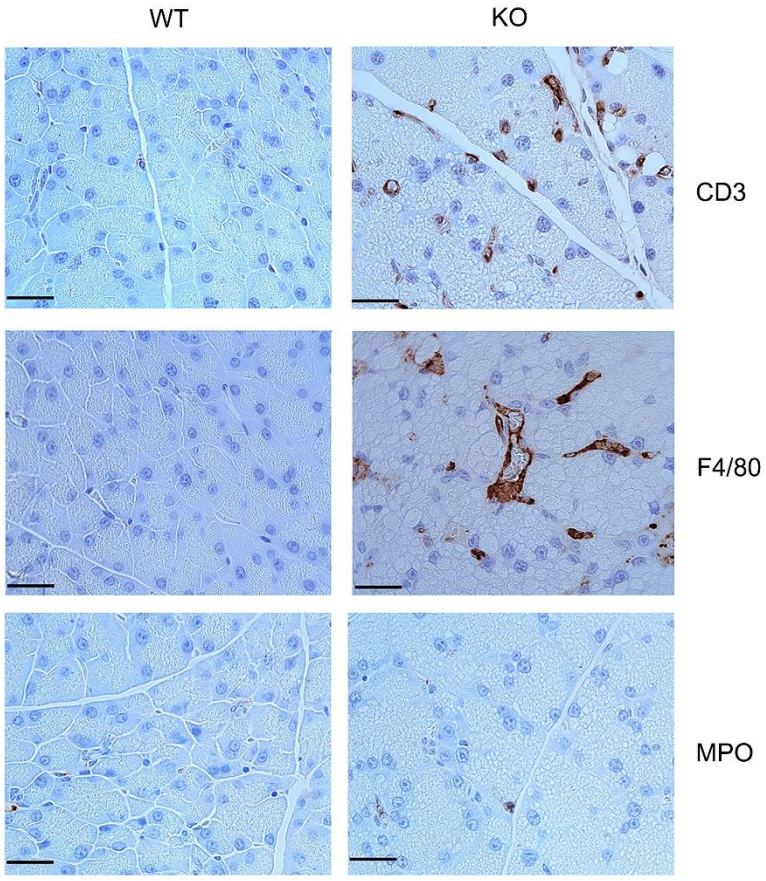

Figure S8. Inflammatory cell infiltration in pancreas of *Gnptab*$^{-/-}$ mice. Representative IHC staining for markers of macrophages (F4/80), neutrophils (myeloperoxidase; MPO), and T-cells (CD3) in WT and KO pancreas. Quantification of these data is shown in Figure 5F.

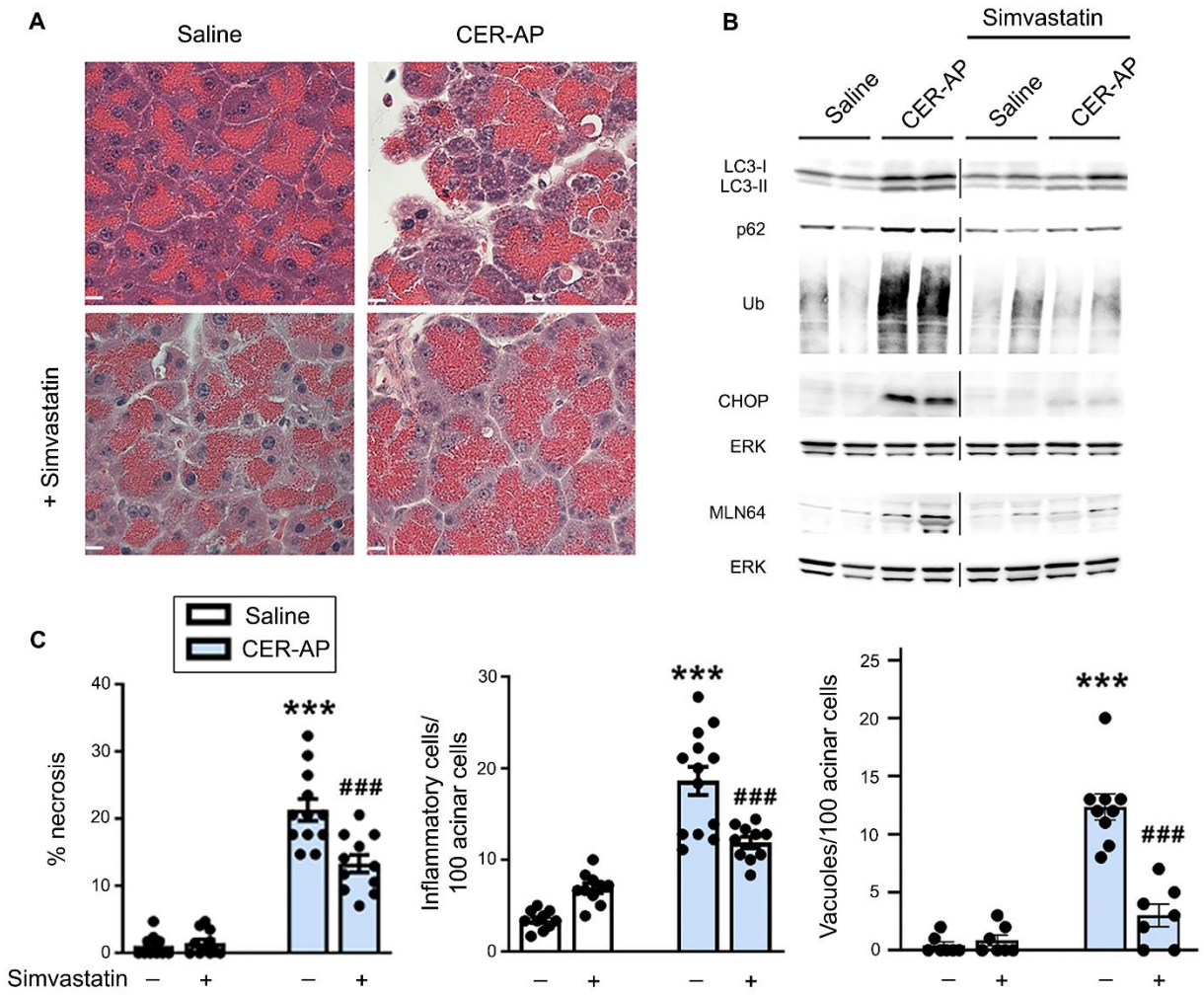

Figure S9. Simvastatin improves cerulein pancreatitis. Mice received daily i.p. injections of simvastatin (Sim; 20 mg/kg) or vehicle (see Figure 10), and on day 4 were subjected to cerulein pancreatitis (CER-AP). (**A**) Pancreas histopathology (H&E staining; scale: 10 µm). (**B**) IB analysis of markers/mediators of autophagy (LC3, p62), ER stress (CHOP), and the MLN64/STARD3 protein mediating cholesterol transfer from LE/Ly to mitochondria. Each IB lane represents an individual mouse; ERK1/2 is the loading control. The narrow black line indicates that lanes are on the same gel but not contiguous. Ub, ubiquitylated proteins. (**C**) Pancreatitis responses. Values are mean ± SEM from 7-13 mice for each condition. ***p<0.001 vs saline control. ###p<0.001 vs CER-AP alone (no simvastatin). Significance was determined by 1-way ANOVA followed by Tukey's multiple comparisons test.